Selecting The Optimal Cross-Section for Control Surface Of Underwater Vehicle

Dr. Purshotham Katti¹, Omkar Bilawar¹, Shreya Agasagi¹, SpoorthiMaracharaddi¹ and Rohit Patil¹

Department of Aeronautical Engineering, KLS Gogte Institute of Technology, Belagavi 590008-, India

Abstract

This abstract summarizes the research topic, objectives, methodology, and expected outcome on Selecting the optimal cross-section for control surfaces for underwater vehicles. This is crucial for achieving efficient manoeuvring and control which also tend to select the aerodynamic shape that produces more lift with less drag. This study investigates the performance of four different aerofoils (i.e., NACA 0012, NACA0006, NACA 0004, and NACA0009) as potential fit for control surfaces in underwater vehicles. The paper employs computational fluid dynamics (CFD) simulations to analyse the hydrodynamic characteristics of each aerofoil, focusing on parameters relevant to control surface performance, such as lift coefficient (Cl), drag coefficient (Cd), and lift-to-drag ratio (Cl/Cd). The study aims to identify the aerofoil that offers the optimal balance between lift generation for maneuverability and low drag for minimizing energy consumption which is also followed by stress analysis, model vibration analysis and their results.

Keywords: CATIA, ANSYS, CFD, FEA, Modal Vibration.

1. Introduction

Selecting Optimal Cross Sections for Control Surfaces in Unmanned Underwater vehicles (UUVs) play a widely crucial role in marine applications as its developing in various field including oceanographic research, resource exploration, Archelogy and defence. This introduction sets the stage for a more detailed discussion on the critical considerations and optimization techniques involved in selecting the optimal cross sections for control surfaces in underwater vehicles [22][23]. It highlights the importance of this design choice for various performance parameters that influence UUV functionality and success in diverse marine applications. Their maneuverability and control are paramount for successful operation, and this heavily relies on the design of their control surfaces

- the fins, rudders, and other appendages used to steer and stabilize the vehicle.[9][11]

Choosing the optimal cross section for these control surfaces is a critical aspect of UUV design. It has a direct impact on various performance parameters, including:

Hydrodynamic efficiency: The shape of the cross-section aerofoil affects water flow and drag forces experienced by the control surface. As an inefficient design [2] can lead to increased energy/power consumption and reduced overall vehicle performance.[1][2][3].

Manoeuvrability: The effectiveness of control surfaces in generating lift and deflecting water flow depends on their cross-sectional shape [27]. Choosing the right shape ensures the UUV can execute desired manoeuvres with precision and agility.

Structural integrity: The cross section needs to be robust enough to withstand the forces exerted by water during operation and while minimizing weight and bulk [15][17][18], as Underwater vehicles often operate in depth where buoyancy is limited.

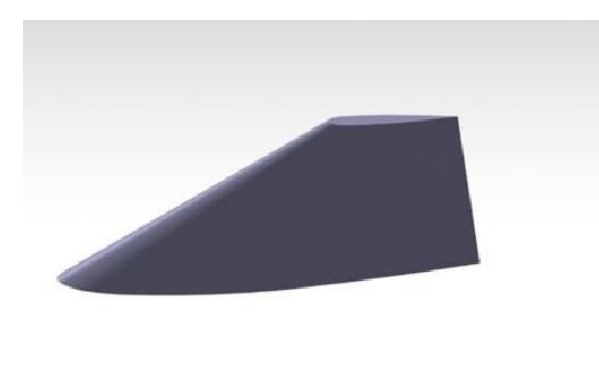
2. Methodology

This methodology is to provides a complete framework for optimizing the design of control surface for

Autonomous underwater vehicle (AUV's) by leveraging the complementary strengths of CFD, FEA, and Model vibration analysis. [27][28]

2.1 Geometry Creation:

This part describes the process of creating different airfoil-based control surface geometries in CATIA V5. Here the required data was taken from airfoil.com website further on the generating control surface shapes using various design tools within CATIA V5. Creating multiple design iterations allows to explore a broader range of potential solutions within the varying cross-sectional shapes for comparison. This is crucial because the optimal solution might not be readily apparent from the outset. By exploring various shapes and dimensions, you increase the chances of finding a design that surpasses the performance of an initial guess.



φ121.04 2389.62

Fig 2.1: Control surface Geometry

Fig 2.1.1: Dimensions of control surface

2.1.2 Mesh generation:

Ansys Meshing provides general-purpose, high-performance, automated, and intelligent meshing software for finite element analysis (FEA) and computational fluid dynamics (CFD) simulations.[25]

2.2 CFD - Computational Fluid Dynamics

2.2.1 CFD Setup:

The steps involved in setting up CFD simulation in ANSYS for each control surface geometries are: The solvers used to get CFD results is K-Epsilon with second order realizable turbulent flow.

The computational domain consists of water with its normal sea level conditions with which is incompressible flow.

Boundary conditions:

• Inlet Velocity: 10.5 m/s

The control surface material is Carbon Fiber

2.2.2 Simulation and Analysis:

After selecting the solver and setting the required parameters like defining the boundary condition the plot must be defined to get the required graph, now click on initialization to start the calculation and after that proceed with clicking on run to get the results.

Pressure distribution: The pressure distribution on the control surface is to understand and analyse the lift and drag forces.[3][28]

1. NACA-0004:

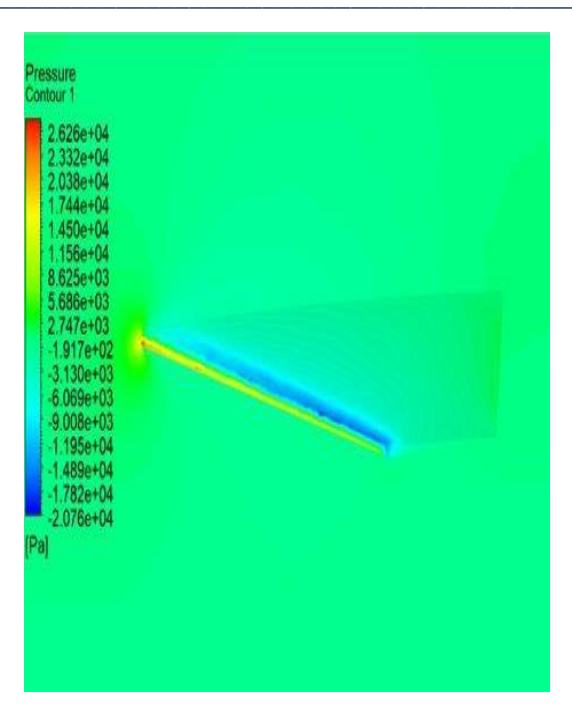


Fig 2.2.1: NACA-0004cross-section control surface

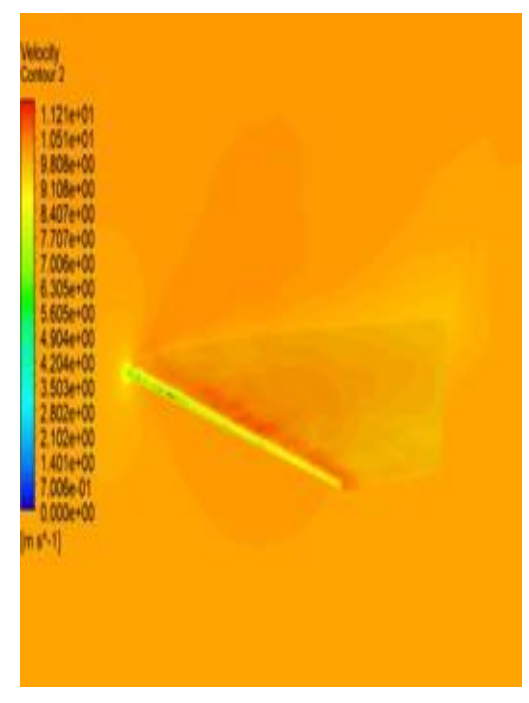
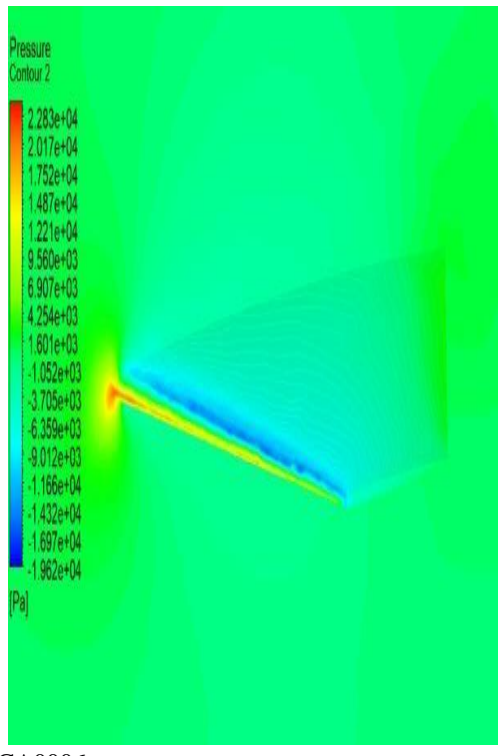


Fig2.2.2 NACA-0004 cross section control surface velocity contour



2. NACA0006:

Fig 2.2.3: NACA-0006 cross section control surface Pressure contour.

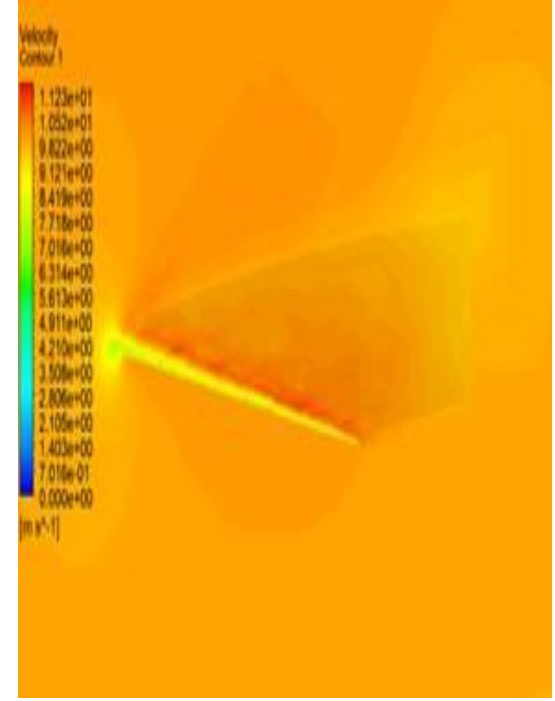


Fig 2.2.4 NACA-0006 cross section control surface velocity contour

NACA-0009

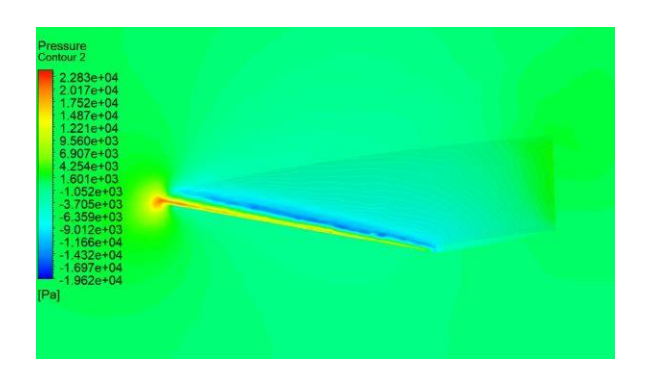


Fig 2.2.3: NACA-0009 cross section control surface Pressure contour.

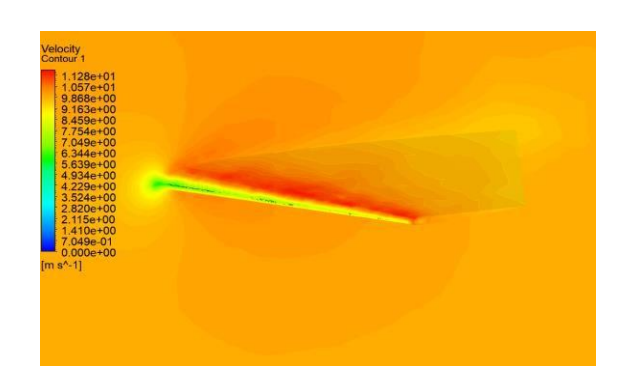


Fig 2.2.4 NACA-0006 cross section control surface velocity contour

4.NACA0012

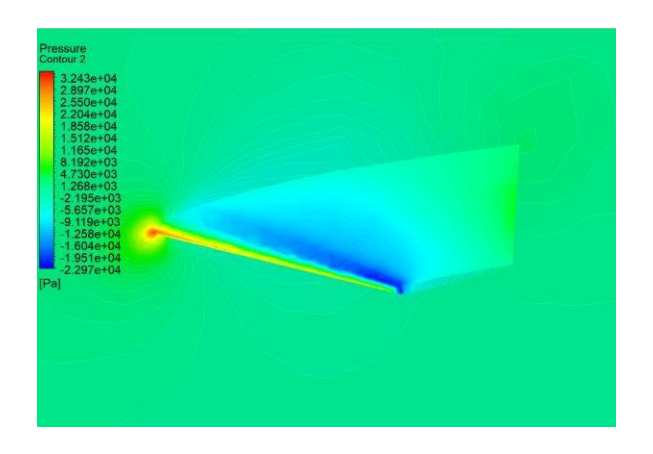


Fig: 2.2.7: NACA-0012 cross section control surface Pressure contour

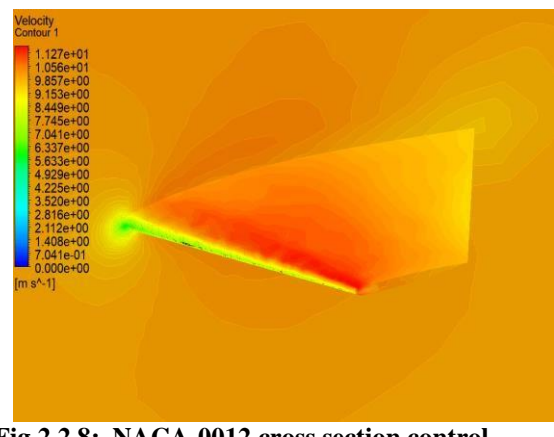


Fig 2.2.8: NACA-0012 cross section control surface Velocity contour

2.3.1 CFD Analysis Results:



The results obtained from various angle of attack at constant free stream velocity for various considered control surfaces are shown in fig 2.2 , from the results we have obtained the Fig 2.3.1: Cl v/s alpha curve , Fig 2.3.2: Cm v/s alpha curve[1][2][3] , Fig 2.3.3: Cl/Cd v/s alpha.

These curves shows the comparison and gives a better idea for functionality and fluid dynamic efficiency for various cross section of control surface.

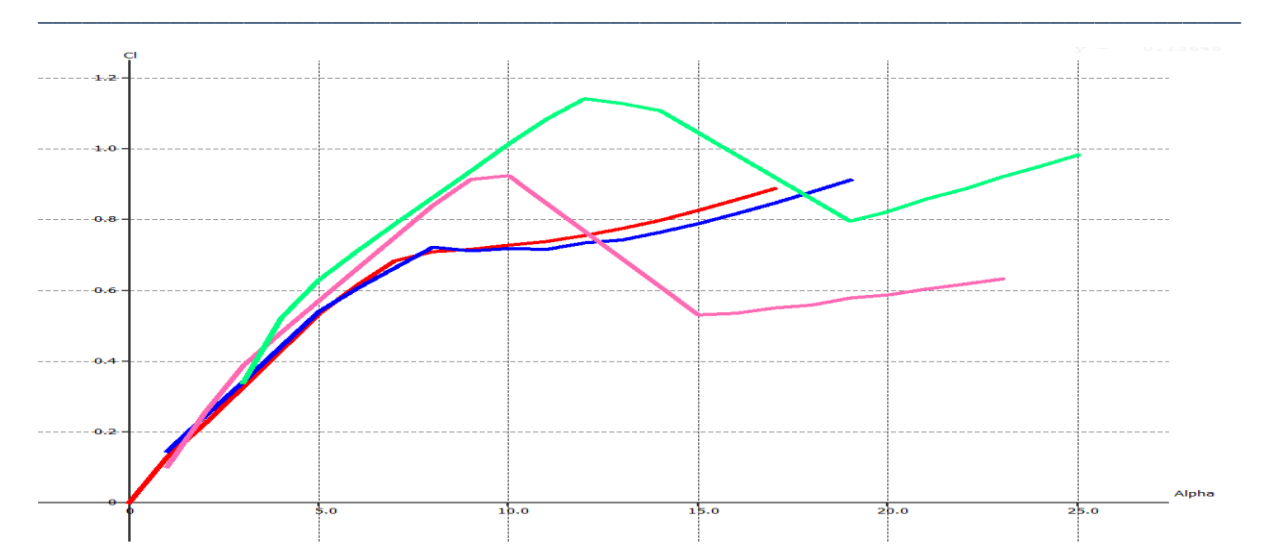


Fig 2.3.1: Cl v/s alpha curve

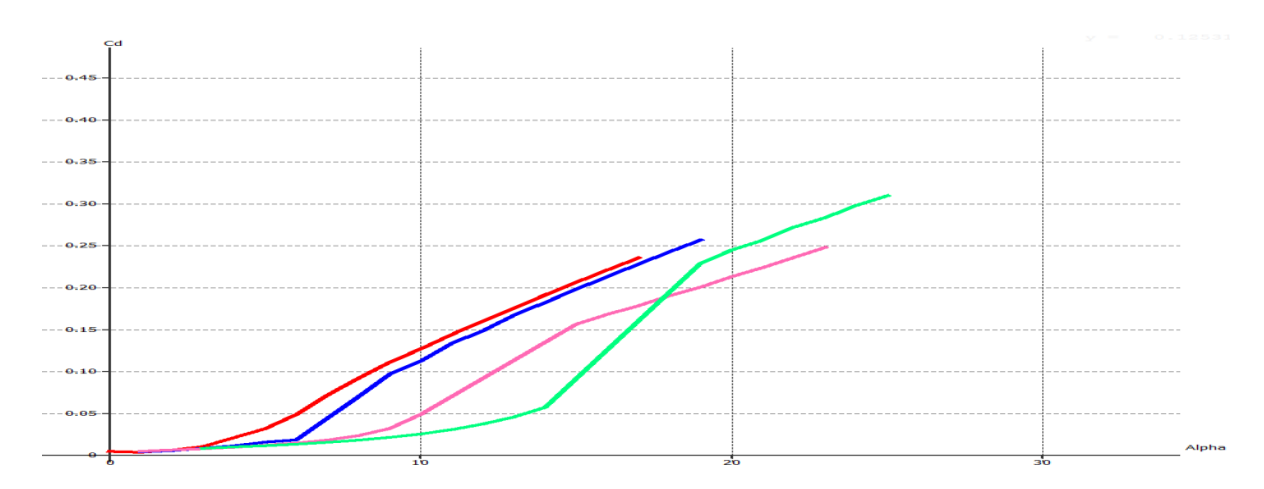


Fig 2.3.2: Cd v/s alpha curve

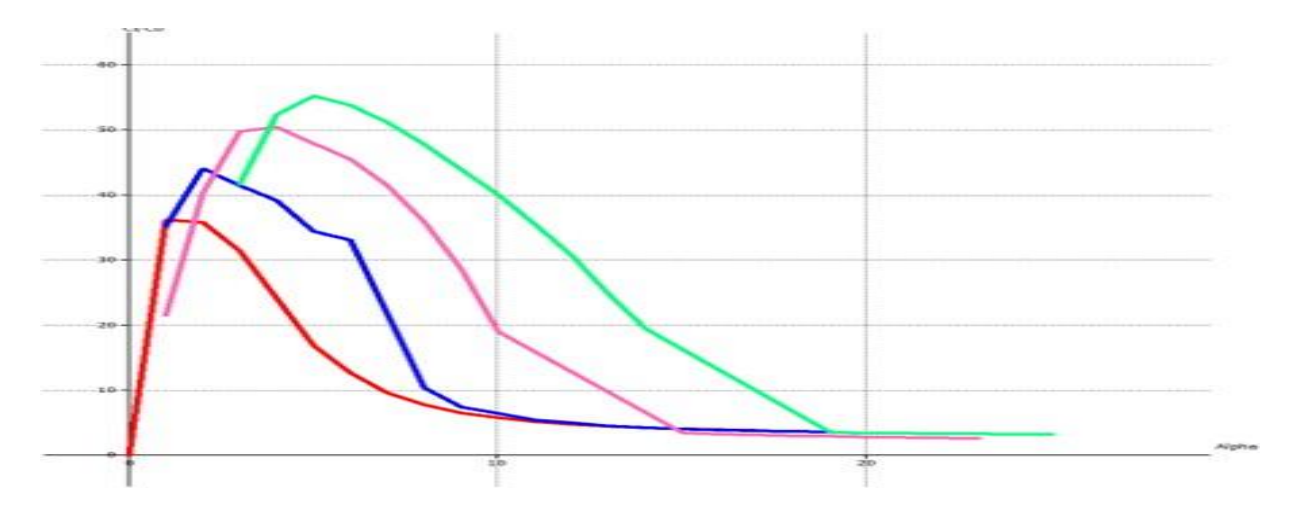


Fig 2.3.3: Cl/Cd v/s alpha.

2.4 FEA-Stress Analysis

Material definition:

Material: Carbon Fiber

• Young's modulus: 395Gpa Loads and Boundary Conditions:

Fixed constraints: Root chord

Dynamic pressure: 60.5 kPa on one side

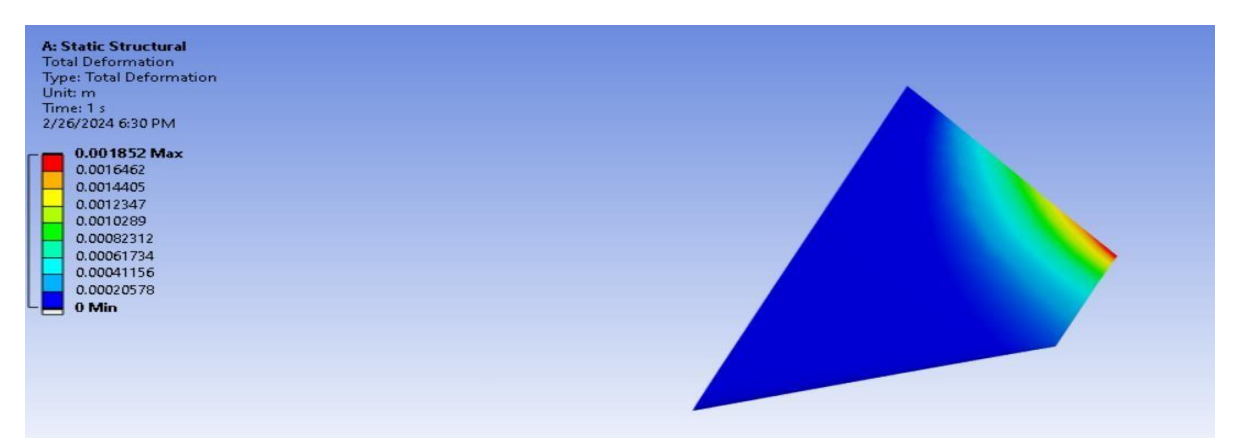


Fig:2.4.1: Total Deformation

Total deformation on the tip signifies that there are no critical areas of structural deformation The total deformation is 0.001852m

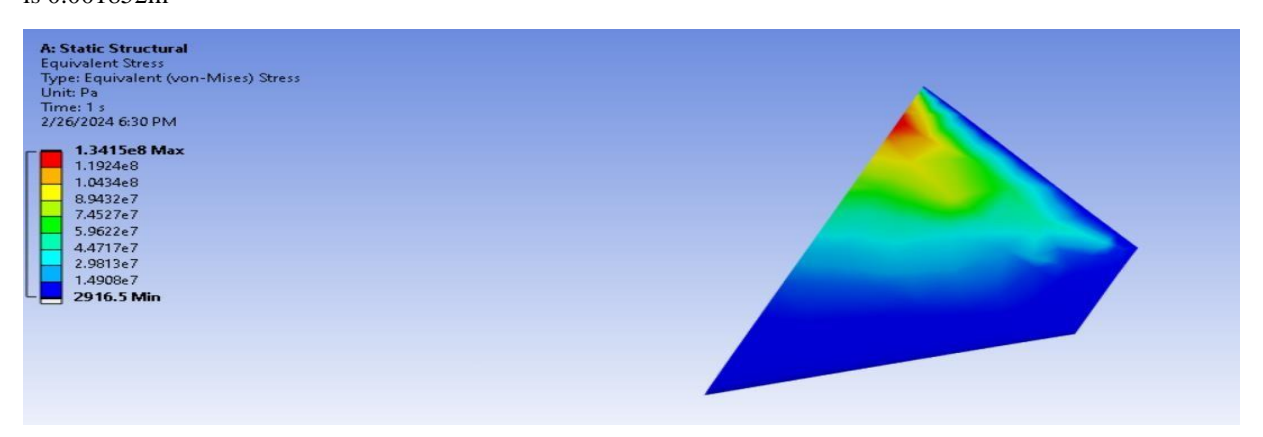


Fig 2.4.2: Equivalent Stress

An Equivalent stress is a measure that combines the normal and shear stresses acting on an object to represent the overall stress intensity. This stress helps to evaluate the structural integrity of components under various loads and conditions. The Equivalent stress obtained is 1.3415*10^8Pa.



Fig 2.4.3: Maximum Principal Stress

Stress distribution is uniform all over the wing body and there is no presence of any critical areas of failure. And the stresses developed are within the proportionality limit[13][14]. Maximum principal stress is the maximum value of normal stress acting on one of the principal planes where the value of shear stress is zero. The maximum principal stress obtained is 1.3254*10^8 Pa. [16][17]

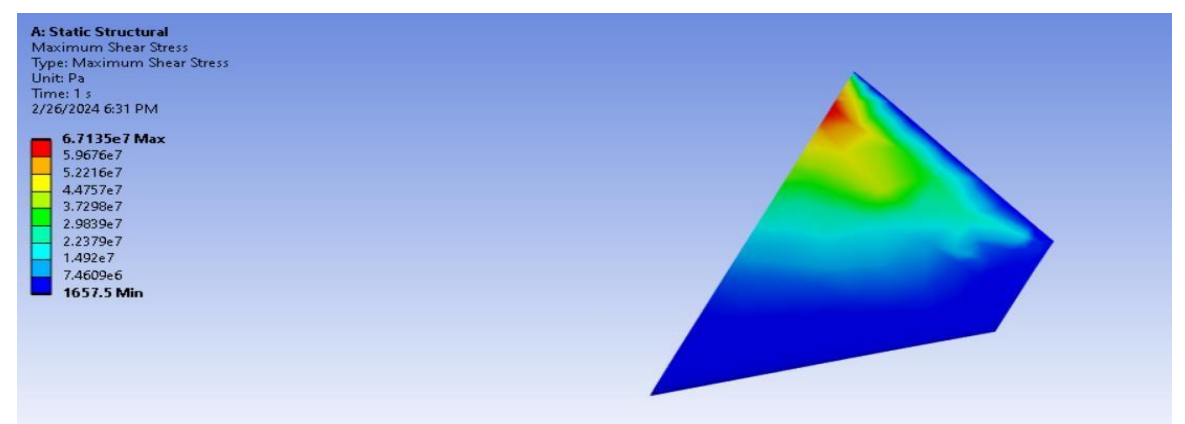


Fig 2.4.4: Maximum Shear Stress The maximum shear stress obtained is 6.714*10^7 Pa.

NACA0006:

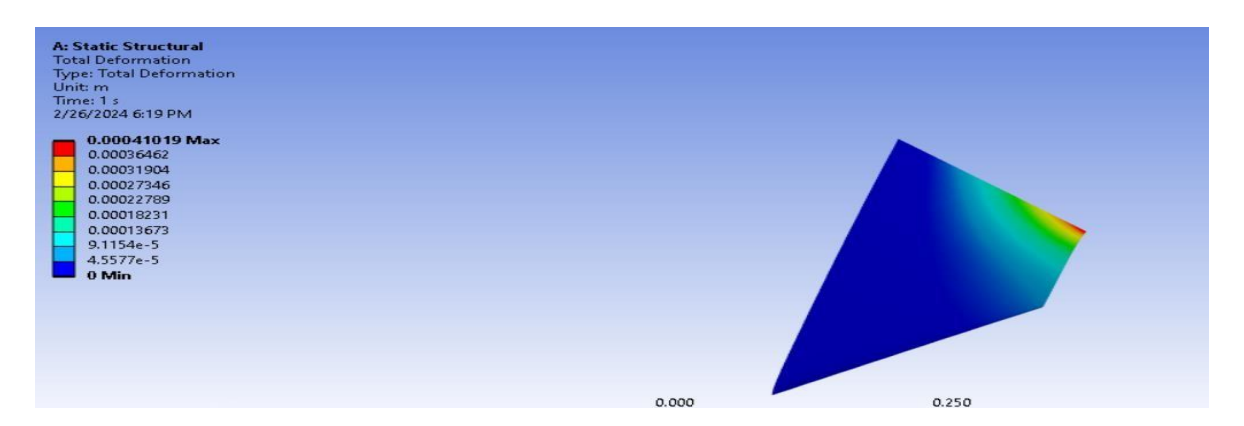


Fig 2.4.5: Total Deformation

Total deformation on the tip signifies that there are no $\,$ critical areas of structural deformation The total deformation is 0.00041019m

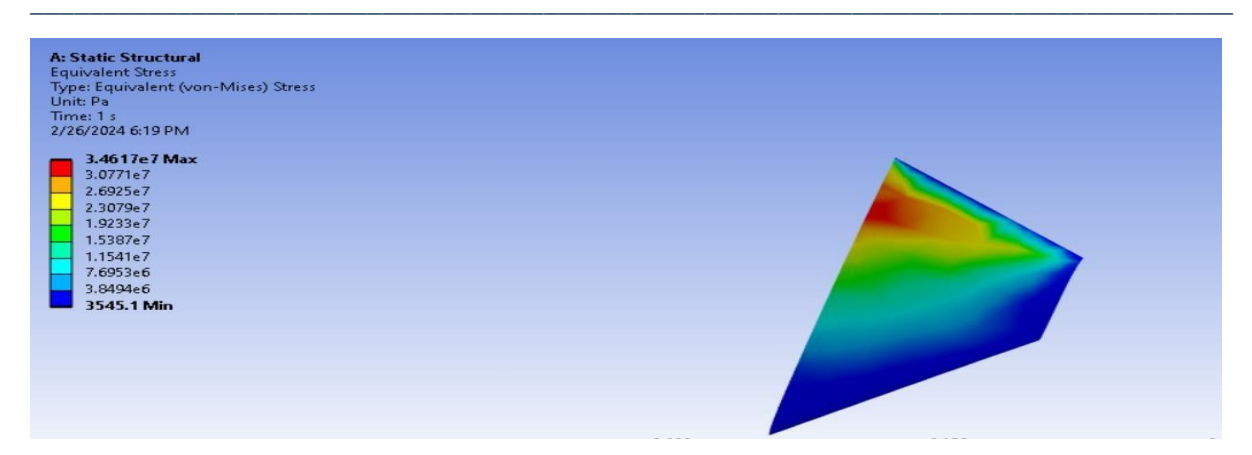


Fig 2.4.6: Equivalent Stress

An Equivalent stress is a measure that combines the normal and shear stresses acting on an object to represent the overall stress intensity. This stress helps to evaluate the structural integrity of components under various loads and conditions. The Equivalent stress obtained is 3.4617*10^7Pa.

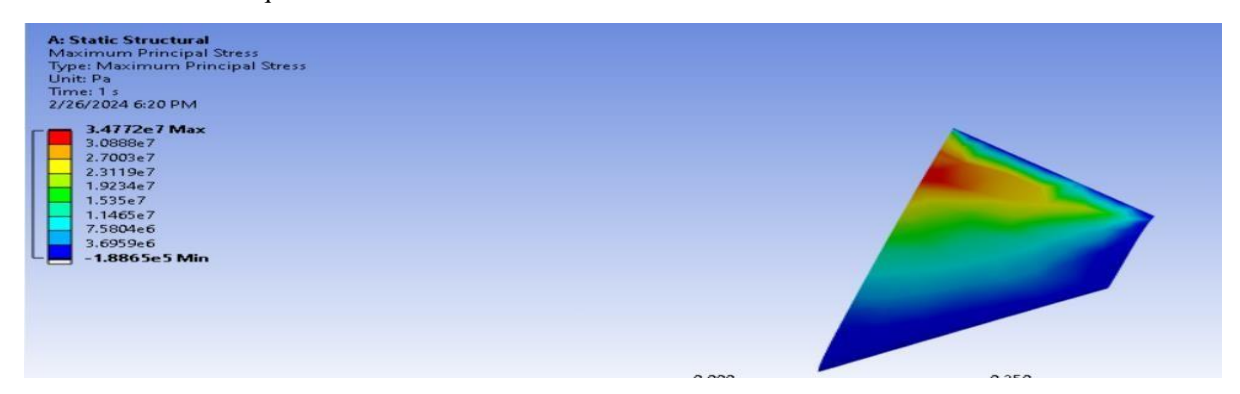


Fig 2.4.7: Maximum Principal Stress

Stress distribution is uniform all over the wing body and there is no presence of any critical areas of failure. And the stresses developed are within the proportionality limit. Maximum principal stress is the maximum value of **normal stress acting on** one of the principal planes where the value of **shear stress** is zero. The maximum principal stress obtained is 3.4772*10^7 Pa.

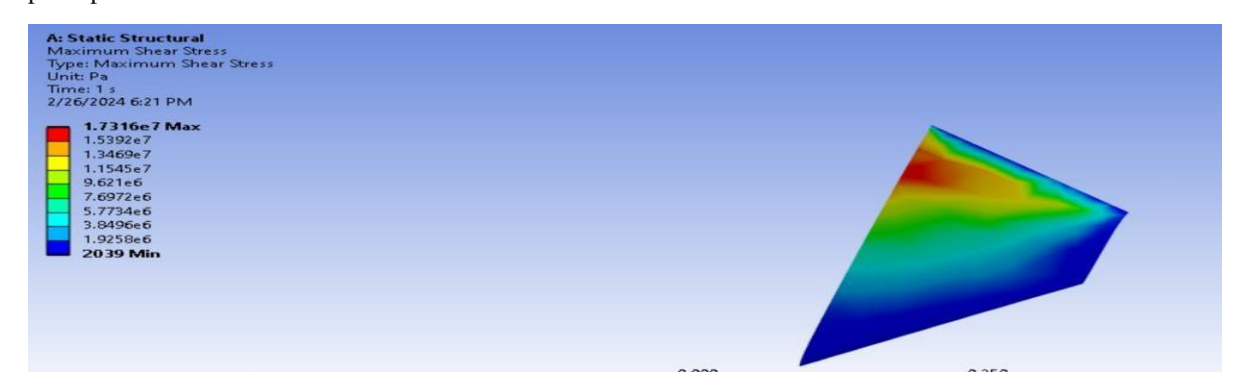


Fig 2.4.8: Maximum Shear Stress The maximum shear stress obtained is 1.735*10^7 Pa.

NACA0009:

Fig 2.4.9: Total Deformation



 $Total\ deformation\ on\ the\ tip\ signifies\ that\ there\ are\ no\ critical\ areas\ of\ structural\ deformation\ The\ total\ deformation\ is\ 0.00049066m$



Fig 2.4.10: Equivalent Stress

An Equivalent stress is a measure that combines the normal and shear stresses acting on an object to represent the overall stress intensity. This stress helps to evaluate the structural integrity of components under various loads and conditions. The Equivalent stress obtained is 4.3466*10^7Pa.

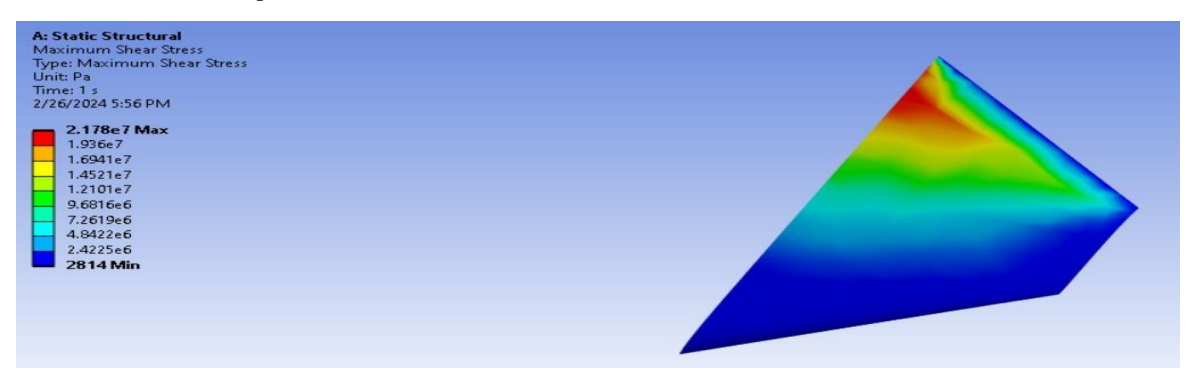


Fig 2.4.11: Maximum Principal Stress

Stress distribution is uniform all over the wing body and there is no presence of any critical areas of failure. And the stresses developed are within the proportionality limit. Maximum principal stress is the maximum value of **normal stress acting on** one of the principal planes where the value of **shear stress** is zero. The maximum principal stress obtained is 2.178*10^7 Pa.

Tuijin Jishu/Journal of Propulsion Technology

ISSN: 1001-4055 Vol. 45 No. 2 (2024)

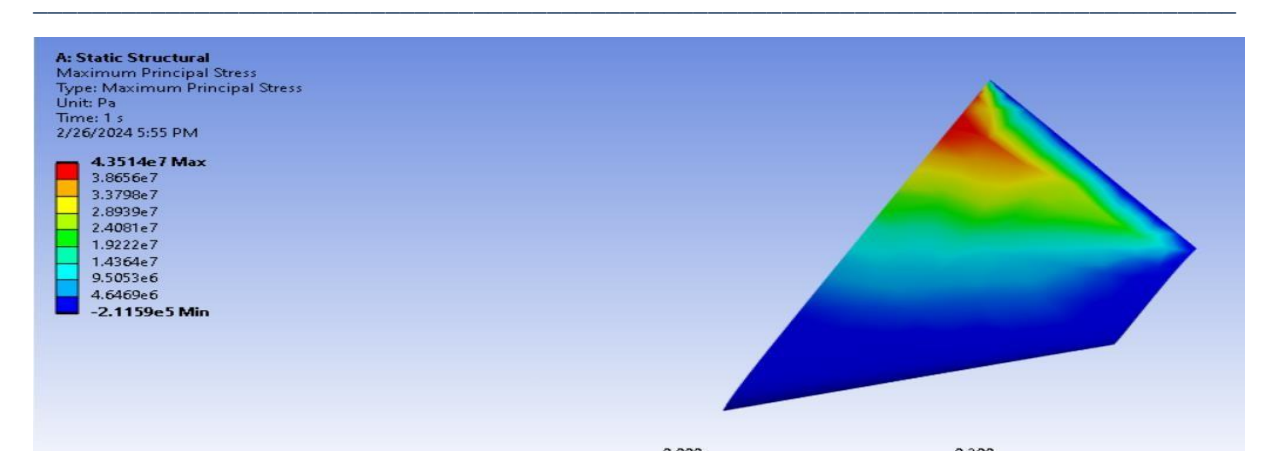


Fig 2.4.12: Maximum Shear Stress The maximum shear stress obtained is 4.351*10^7 Pa.

NACA0012:

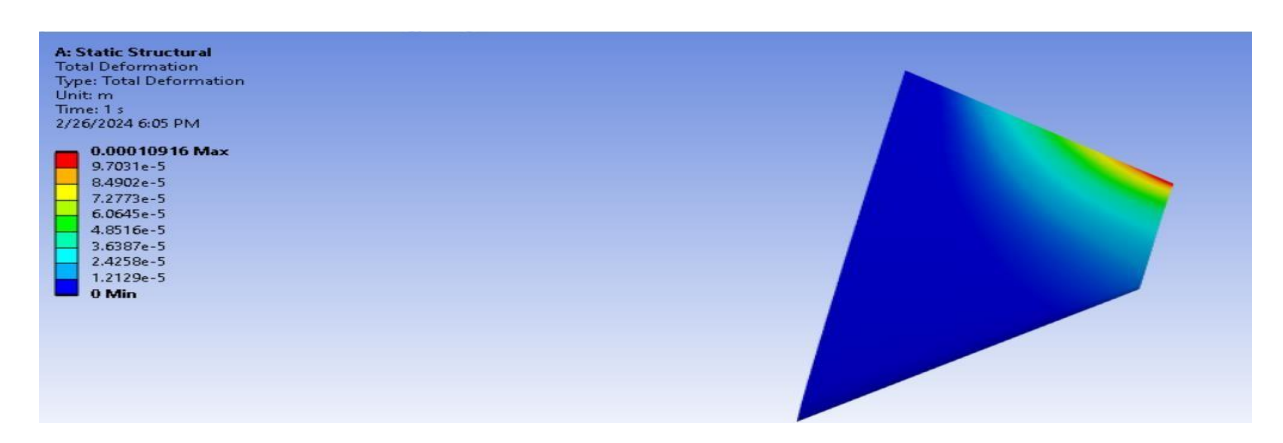


Fig 2.4.13: Total Deformation

Total deformation on the tip signifies that there are no critical areas of structural deformation The total deformation is 0.00010916m



Fig 2.4.14: Equivalent Stress

An Equivalent stress is a measure that combines the normal and shear stresses acting on an object to represent the overall stress intensity. This stress helps to evaluate the structural integrity of components under various loads and conditions. The Equivalent stress obtained is 1.4549*10^7Pa.

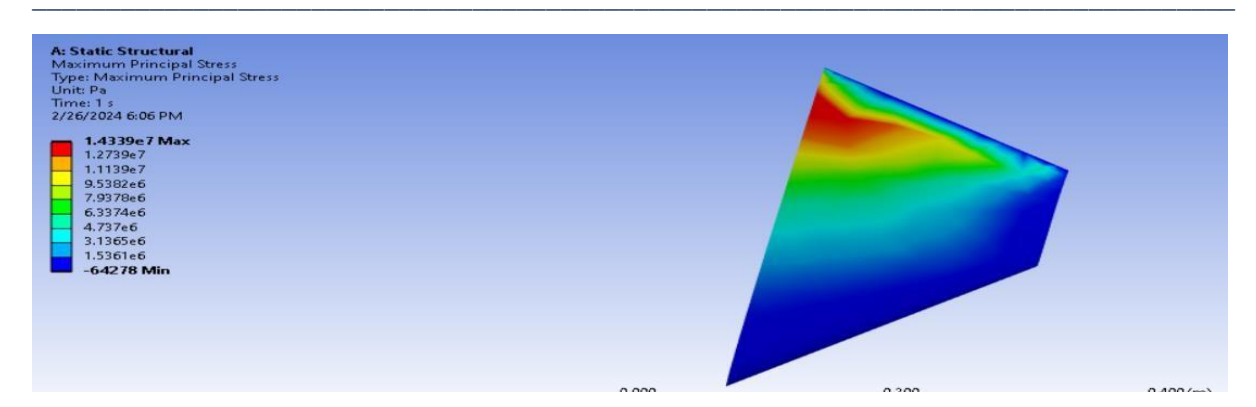


Fig 2.4.15: Maximum Principal Stress

Stress distribution is uniform all over the wing body and there is no presence of any critical areas of failure. And the stresses developed are within the proportionality limit. Maximum principal stress is the maximum value of **normal stress acting on** one of the principal planes where the value of **shear stress** is zero. The maximum principal stress obtained is 1.4339*10^7 Pa.

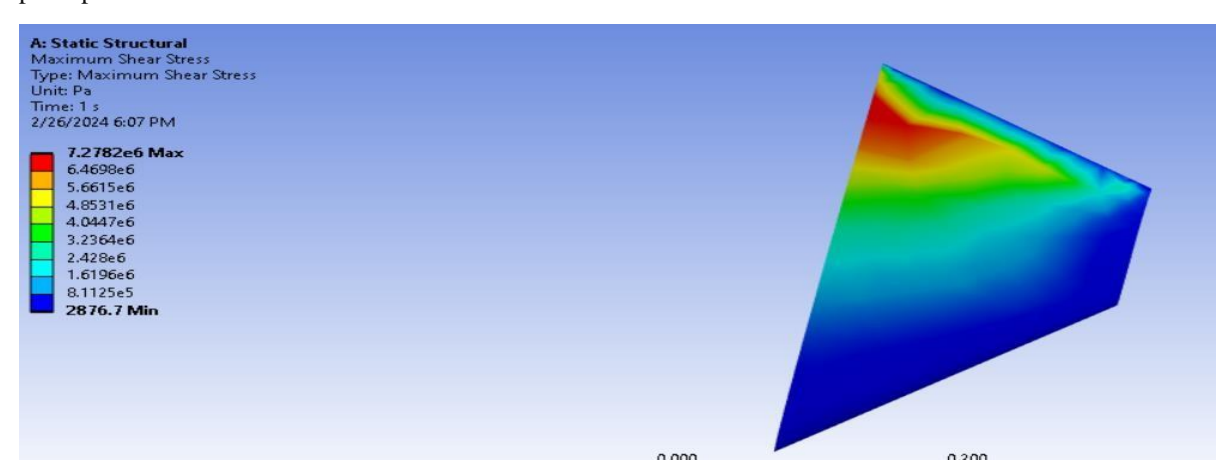


Fig 2.4.16: Maximum Shear Stress The maximum shear stress obtained is 7.278*10^6 Pa.

2.5 Modal Vibration

NACA0004:

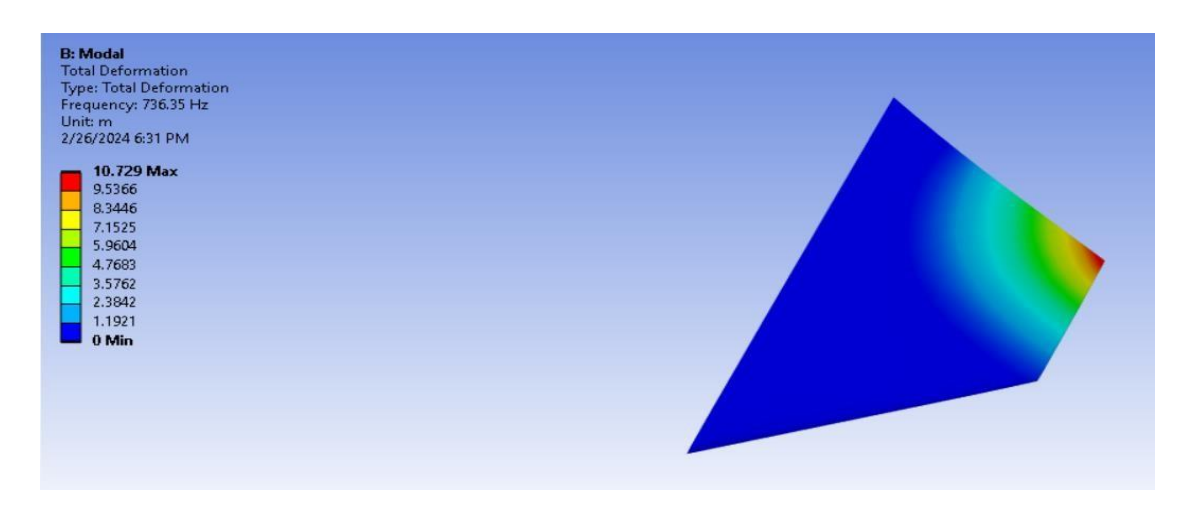


Fig: 2.5.1: Mode 1: Total Deformation 1

Total deformation on the tip signifies that there are no critical areas of structural deformation The total deformation is 10.729m and the frequency is 736.35Hz



Fig 2.5.2: Mode 2: Total Deformation 2

Total deformation on the tip signifies that there are no critical areas of structural deformation The total deformation is 9.7261m and the frequency is 1011.9

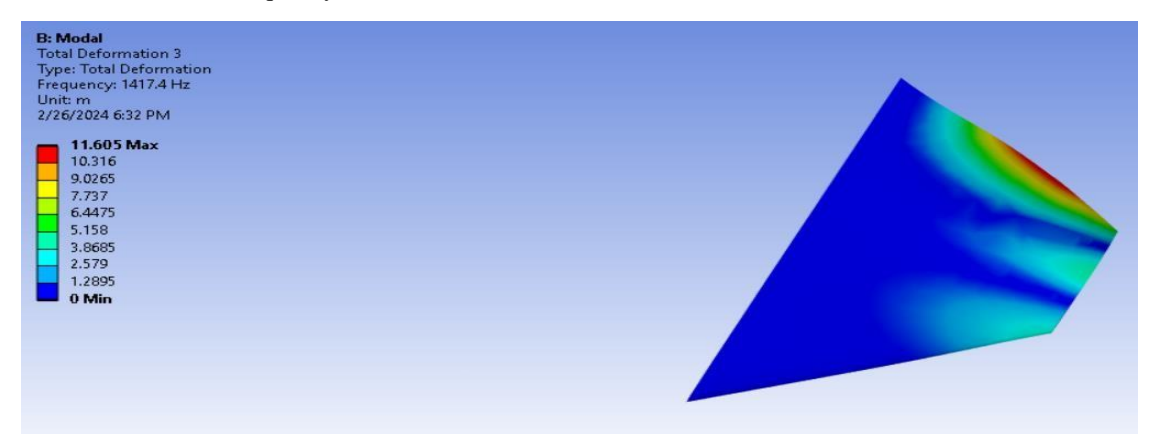


Fig 2.5.3: Mode 3: Total Deformation 3

Total deformation on the tip signifies that there are no critical areas of structural deformation The total deformation is 11.61m and the frequency is 1417.4~Hz



Fig 2.5.4: Mode 4: Total Deformation 4

Total deformation on the tip signifies that there are no critical areas of structural deformation The total deformation is 11.423 and the frequency is 1941.1Hz

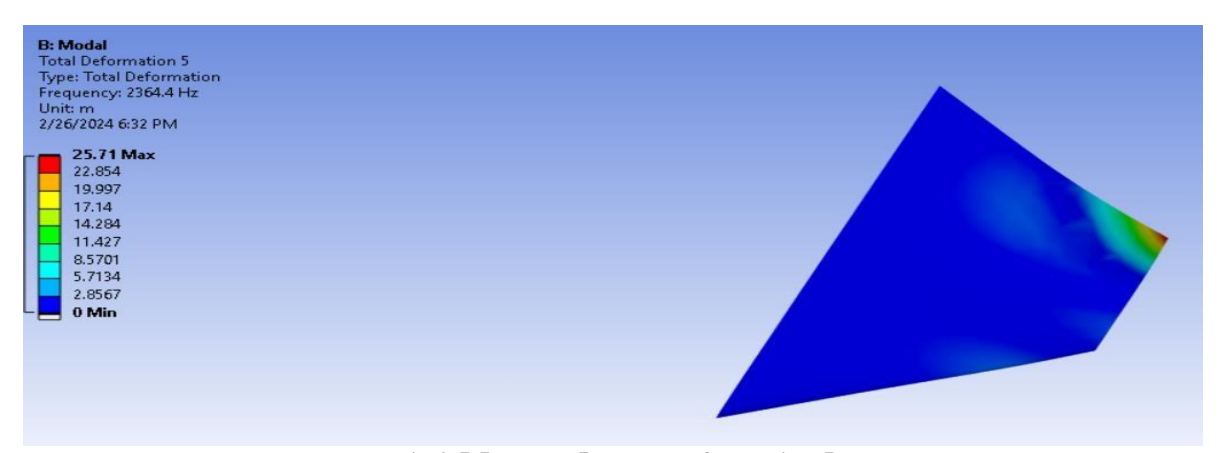


Fig 2.5.5: Mode 5: Total Deformation 5

Total deformation on the tip signifies that there are no critical areas of structural deformation The total deformation is 25.71m and the frequency is 2364.4Hz

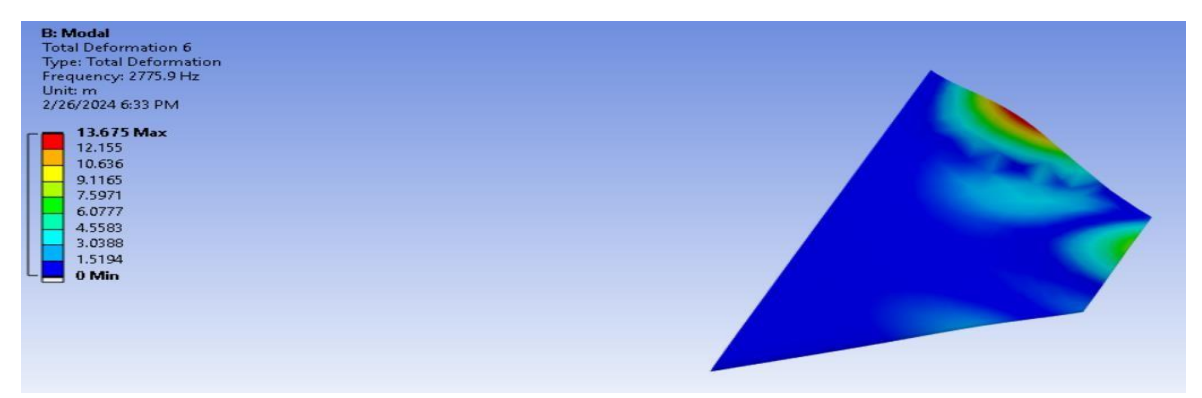


Fig 2.5.6: Mode 6: Total Deformation 6

 $Total \ deformation \ on \ the \ tip \ signifies \ that \ there \ are \ no \ critical \ areas \ of \ structural \ deformation \ The \ total \ deformation \ is \ 13.675 and \ the \ frequency \ is \ 2775.9 Hz$

NACA 0006:

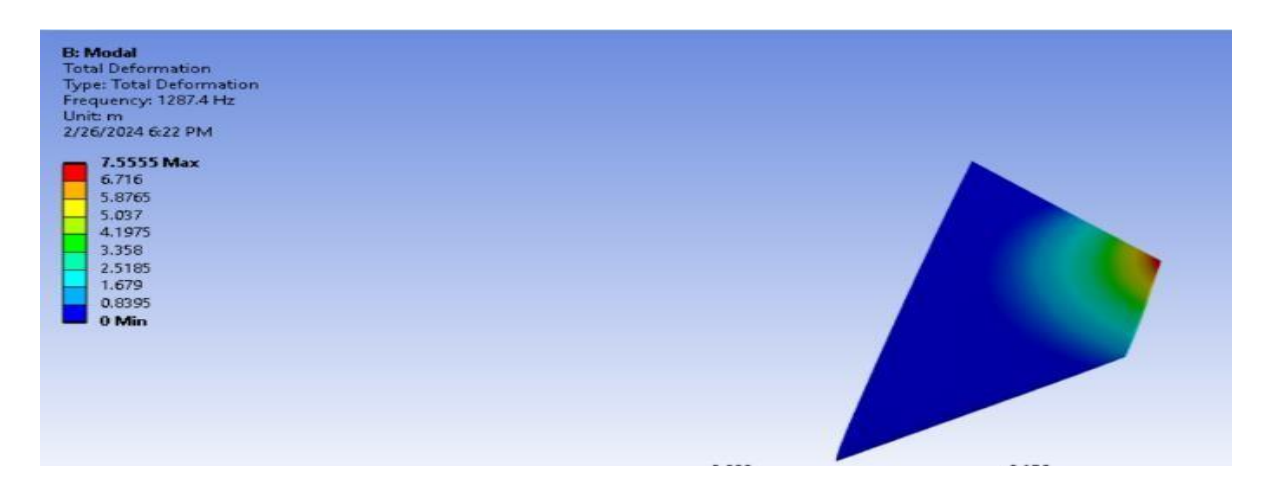


Fig 2.5.7: Mode 1: Total Deformation 1

Total deformation on the tip signifies that there are no critical areas of structural deformation The total deformation is 7.555m and the frequency is 1287.4Hz



Fig 2.5.8: Mode 2: Total Deformation 2

Total deformation on the tip signifies that there are no critical areas of structural deformation The total deformation is 9.333m and the frequency is 1622.4Hz

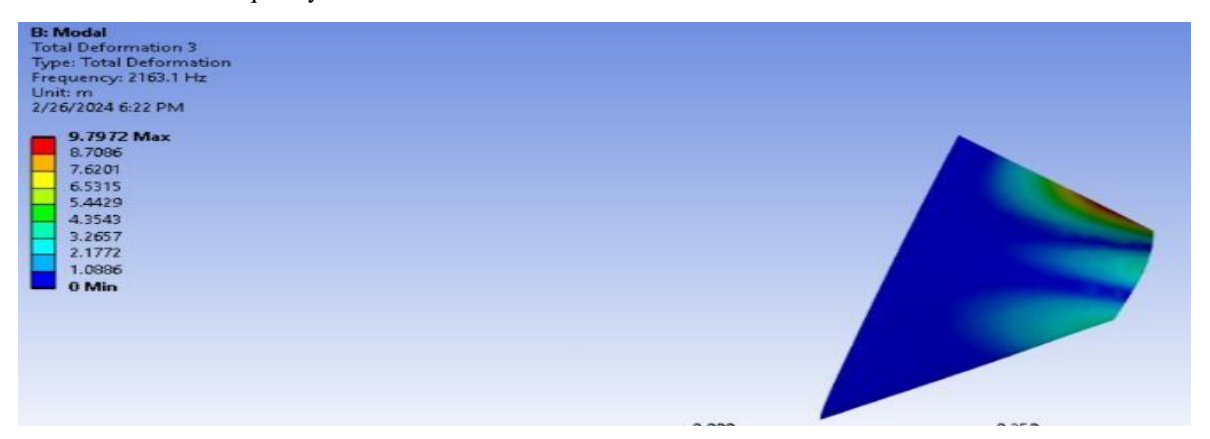


Fig 2.5.9: Mode 3: Total Deformation 3

 $Total \ deformation \ on \ the \ tip \ signifies \ that \ there \ are \ no \ critical \ areas \ of \ structural \ deformation \ The \ total \ deformation \ is \ 9.797m \ and \ the \ frequency \ is \ 2163.1Hz$

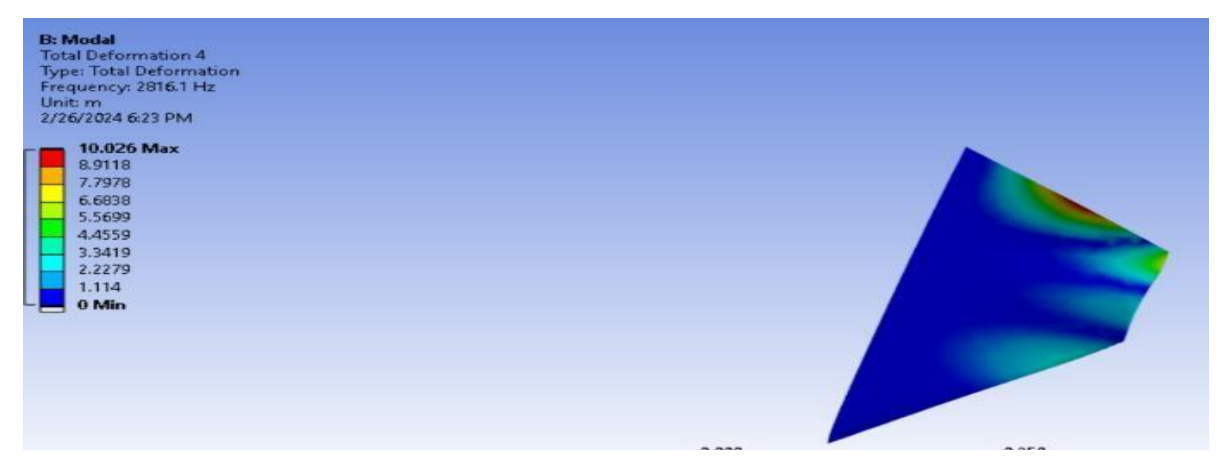


Fig 2.5.10: Mode 4: Total Deformation 4

Total deformation on the tip signifies that there are no critical areas of structural deformation The total deformation is 10.03m and the frequency is 2816.1Hz

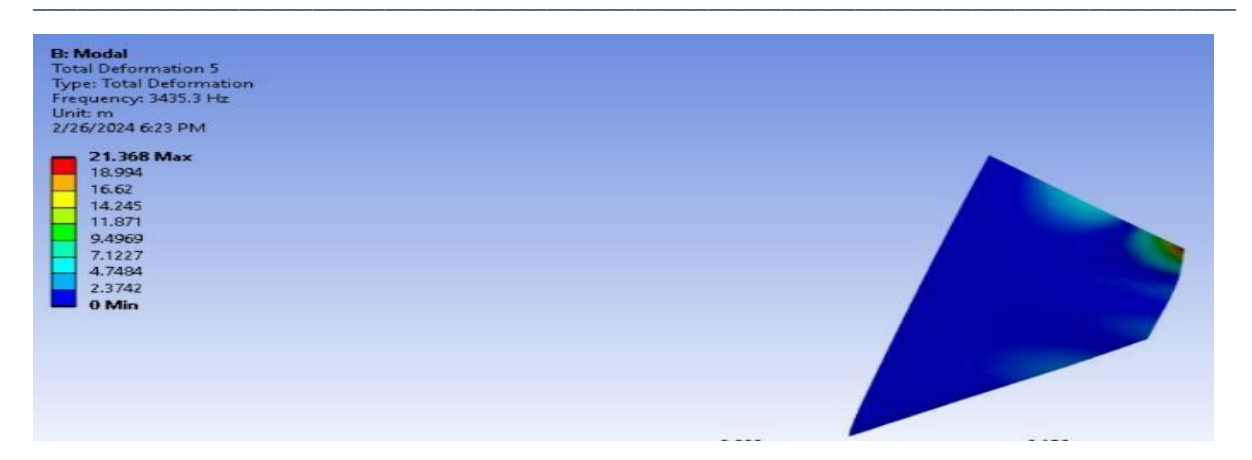


Fig 2.5.11: Mode 5: Total Deformation 5

 $Total \ deformation \ on the \ tip \ signifies \ that \ there \ are \ no \ critical \ areas \ of \ structural \ deformation \ The \ total \ deformation \ is \ 21.37m \ and \ the \ frequency \ is \ 3435.3Hz$

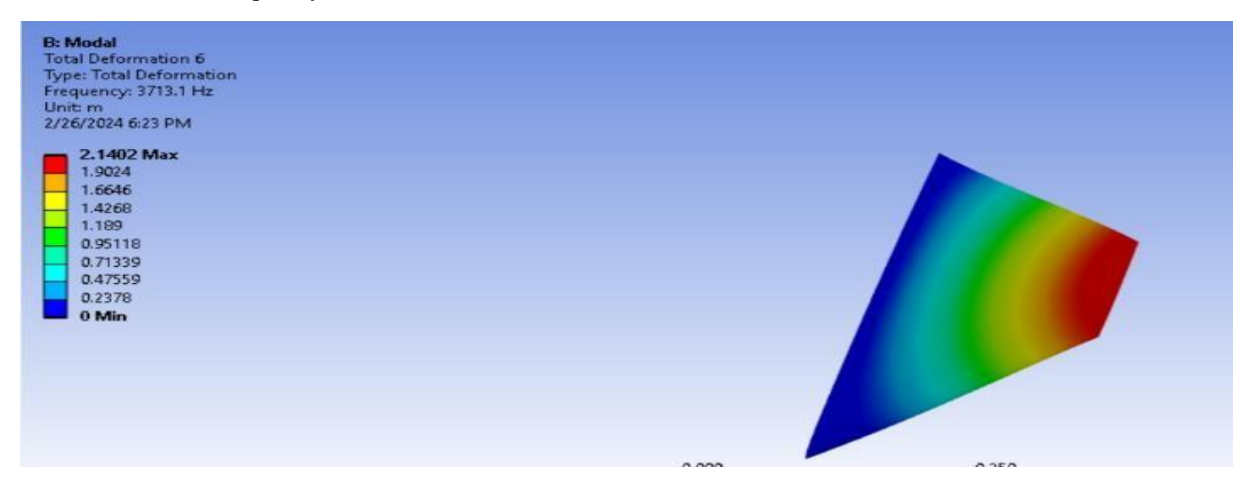


Fig 2.5.12: Mode 6: Total Deformation 6

Total deformation on the tip signifies that there are no critical areas of structural deformation The total deformation is 2.14m and the frequency is 3713.1Hz

NACA 0009:

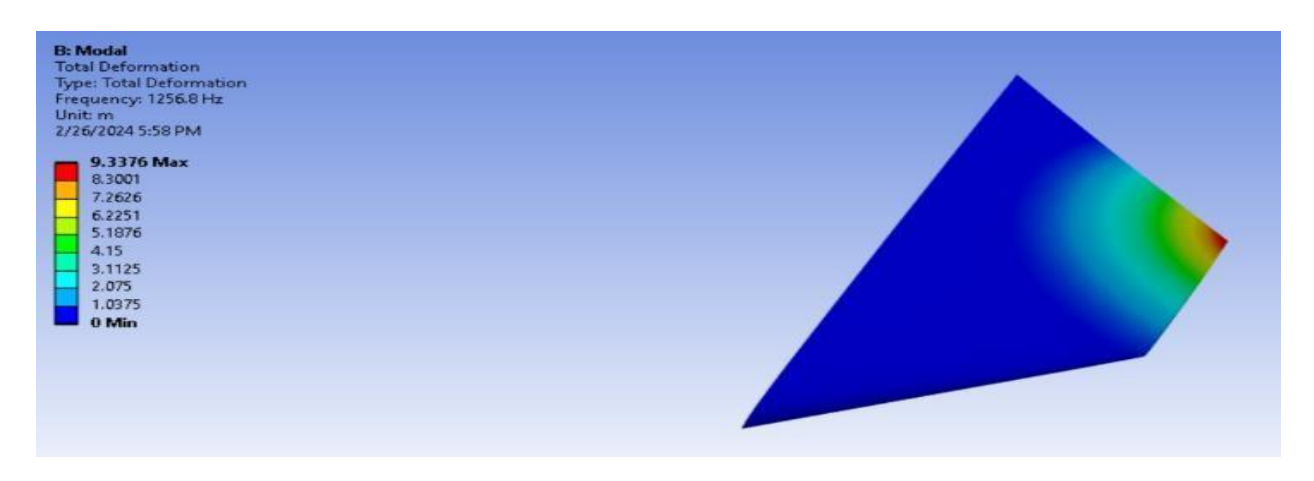


Fig 2.5.13: Mode 1: Total Deformation 1

Total deformation on the tip signifies that there are no critical areas of structural deformation The total deformation is 9.338m and the frequency is 1256.8Hz



Fig 2.5.14: Mode 2: Total Deformation 2

Total deformation on the tip signifies that there are no critical areas of structural deformation The total deformation is 9.602m and the frequency is 1639.9Hz

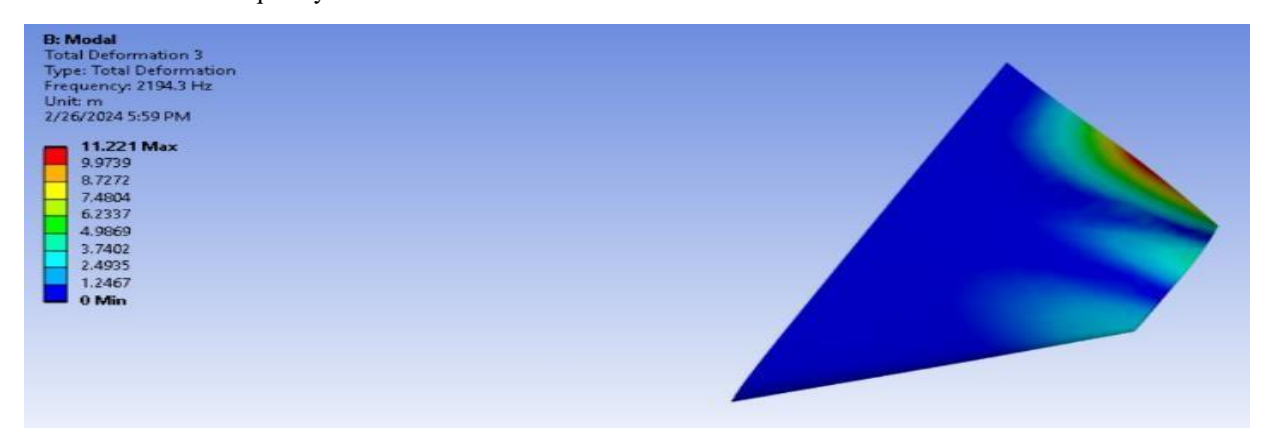


Fig 2.5.15: Mode 3: Total Deformation 3

Total deformation on the tip signifies that there are no critical areas of structural deformation The total deformation is 11.22m and the frequency is 2194.3Hz



Fig 2.5.16: Mode 4: Total Deformation 4

Total deformation on the tip signifies that there are no critical areas of structural deformation The total deformation is 12.27m and the frequency is 2803.8Hz

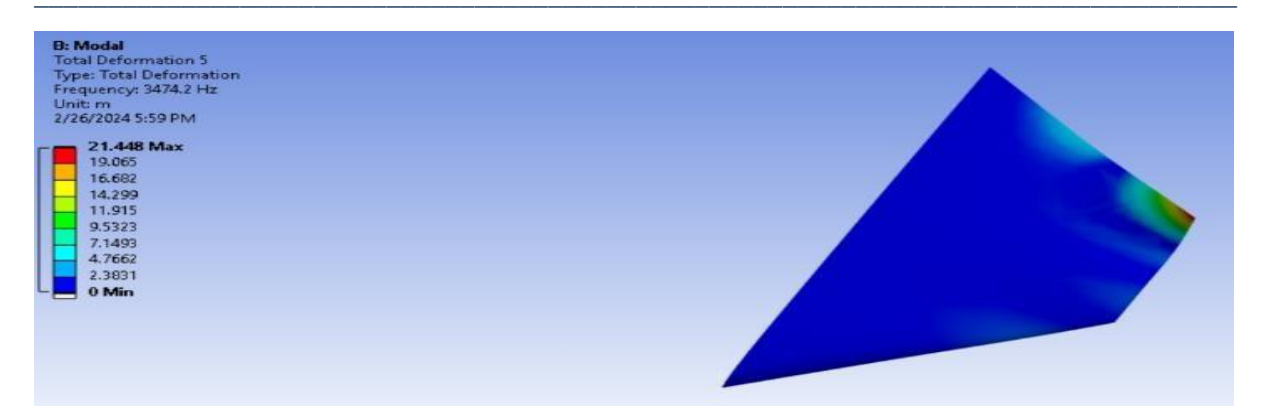


Fig 2.5.17: Mode 5: Total Deformation 5

 $Total\ deformation\ on\ the\ tip\ signifies\ that\ there\ are\ no\ critical\ areas\ of\ structural\ deformation\ The\ total\ deformation\ is\ 21.45m\ and\ the\ frequency\ is\ 3474.2Hz$



Fig 2.5.18: Mode 6: Total Deformation 6

 $Total \ deformation \ on \ the \ tip \ signifies \ that \ there \ are \ no \ critical \ areas \ of \ structural \ deformation \ The \ total \ deformation \ is \ 1.986m \ and \ the \ frequency \ is \ 3.679.1 Hz$

NACA 0012:

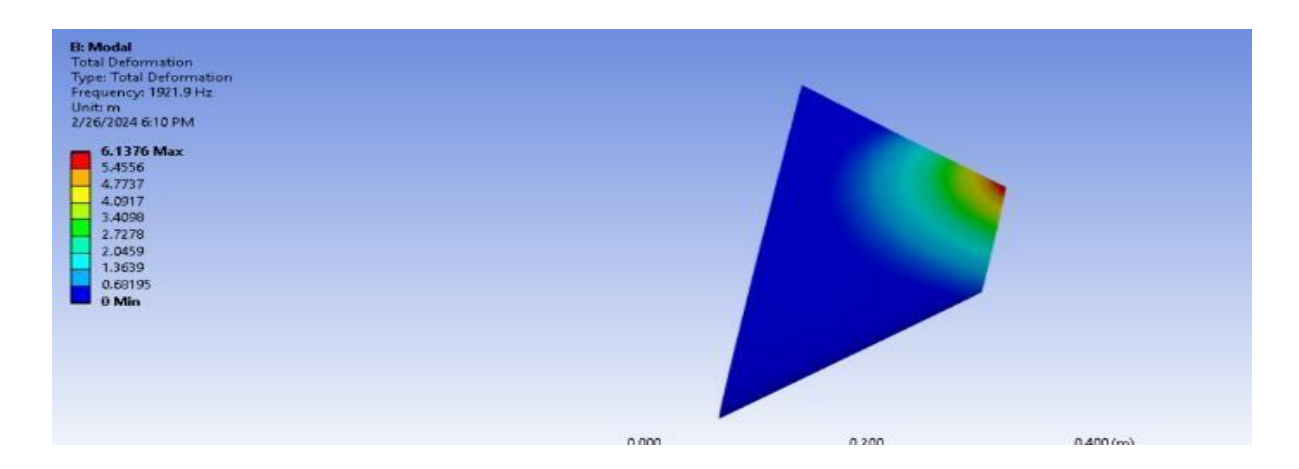


Fig 2.5.19: Mode 1: Total Deformation 1

Total deformation on the tip signifies that there are no critical areas of structural deformation The total deformation is 6.138m and the frequency is 1921.9Hz



Fig 2.5.20: Mode 2: Total Deformation 2

Total deformation on the tip signifies that there are no critical areas of structural deformation The total deformation is 6.59m and the frequency is 2448.6Hz

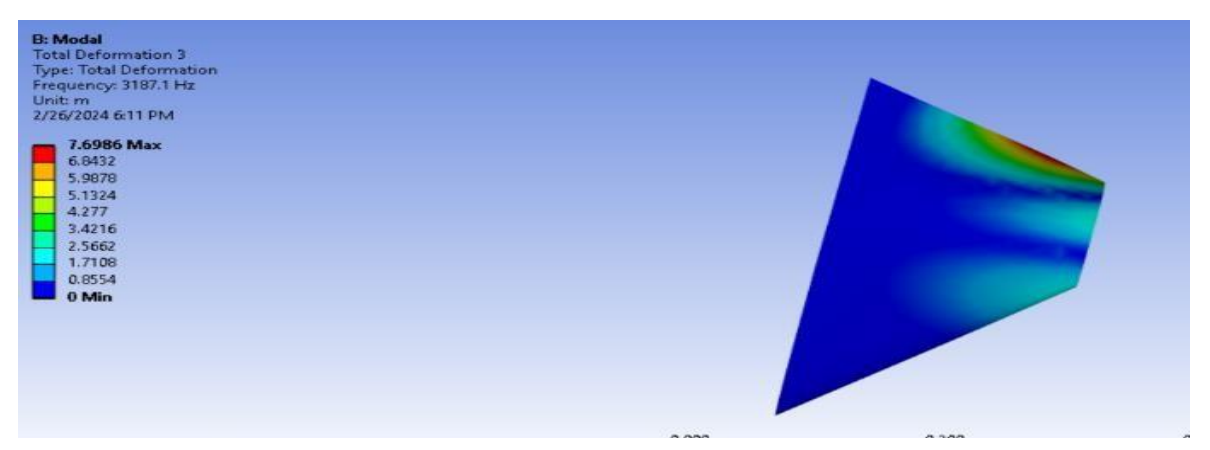


Fig 2.5.21: Mode 3: Total Deformation 3

Total deformation on the tip signifies that there are no critical areas of structural deformation The total deformation is 7.699m and the frequency is 3187.1Hz



Fig 2.5.22: Mode 4: Total Deformation 4

 $Total \ deformation \ on \ the \ tip \ signifies \ that \ there \ are \ no \ critical \ areas \ of \ structural \ deformation \ The \ total \ deformation \ is \ 1.628m \ and \ the \ frequency \ is \ 3710.4Hz$



Fig 2.5.23: Mode 5: Total Deformation 5

 $Total \ deformation \ on \ the \ tip \ signifies \ that \ there \ are \ no \ critical \ areas \ of \ structural \ deformation \ The \ total \ deformation \ is \ 8.679m \ and \ the \ frequency \ is \ 3980.3Hz$



Fig 2.5.24: Mode 6: Total Deformation 6

Total deformation on the tip signifies that there are no critical areas of structural deformation The total deformation is 14.27m and the frequency is 4723.3Hz

4. Result:

The obtained results from static loading effects and modal vibration are clubbed together to showcase the maximum deformation and resonance frequency of vibration as shown in Fig.4.1 and Fig.4.2.

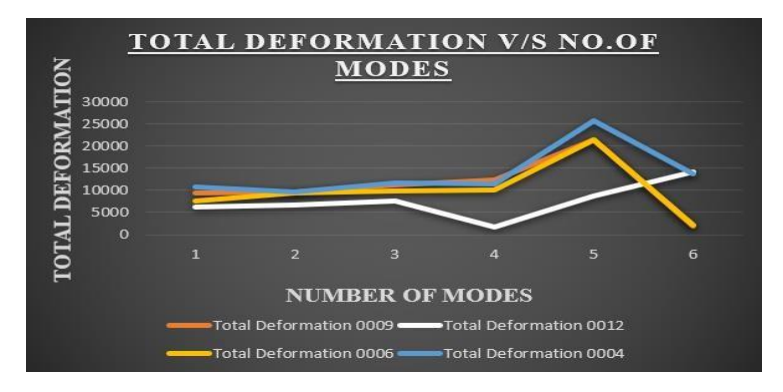


Fig 4.1: Total Deformation (in mm) v/s No. of modes

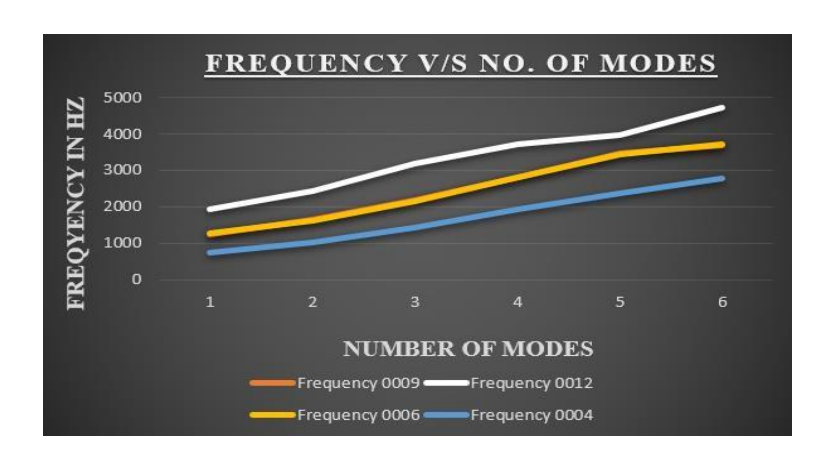


Fig 4.2: Frequency v/s No. of modes

MODE	<u>Total</u>	<u>Total</u>	<u>Total</u>	<u>Total</u>
	Deformation	Deformation	Deformation	Deformation
	0009	0012	<u>0006</u>	<u>0004</u>
1	9337.6	6137.6	7555.5	10729
2	9601.8	6594.8	9332.5	9726.1
3	11221	7698.6	9797.2	11605
4	12265	1627.9	10026	11423
5	21448	8678.7	21368	25710
6	1986.1	14266	2140.2	13675

Table1. Stress analysis data

MODE	FREQUENCY	FREQUENCY	FREQUENCY	FREQUENCY
	0009	0012	0006	<u>0004</u>
1	1256.8	1921.9	1287.4	736.35
2	1639.9	2448.6	1622.4	1011.9
3	2194.3	3187.1	2163.1	1417.4
4	2803.8	3710.4	2816.1	1941.1
5	3474.2	3980.3	3435.3	2364.4
6	3679.1	4723.3	3713.1	2775.9

Table 2. Modal analysis data.

5.Conclusion:

Considering the results obtained after the above numerical solutions we can conclude the fluid dynamic efficiency decreases with increasing thickness and the structural strength increases with thickness to tackle the hydrodynamic pressure considered for mission profile.[28][29] The optimal selection based on the mission requirement will be NACA-0006 which remains in the moderate range in terms of fluid dynamic efficiency and static loading scenario.

Tuijin Jishu/Journal of Propulsion Technology

ISSN: 1001-4055 Vol. 45 No. 2 (2024)

REFERENCES

- [1] Khademzadeh, S. M., & Teimouri, M. 2016. "Design optimization of a flapping foil section for an underwater vehicle using CFD simulations". *Ocean Engineering*, 123
- [2] Liu Y., Wang H., & He M. 2019 "Shape optimization of a wave glider control fin using a hybrid optimization method". *Ocean Engineering*, 187
- [3] Wu G., Xu H., & Liu Z. 2015 "Multi-objective optimization design of an AUV stern using a hybrid method of CFD and surrogate model". *Ocean Engineering*, 110, 174-185.
- [4] Gülten A., & Özkan S. 2018 "Hydrodynamic analysis of a high-performance control surface for an AUV using RANS method". *Ocean Engineering*, 164, 302-312.
- [5] Zhang D., Ye M., & Wang J. 2013 "Hydrodynamic optimization design for a wave glider control fin using response surface methodology" *Ocean Engineering*, 71, 178-188.
- [6] Moheb Mahmoudzadeh Shirazi, Amir Hossein Alasty, Siamak Yasakli 2020 "A Review of Hydrodynamic Design Optimization Techniques for Underwater Vehicles" *The Journal of Engineering for the Maritime Environment*.
- [7] Sverdrup-Thygeson J, Kelasidi E, Pettersen KY 2016 "The underwater swimming manipulator—a bio-inspired AUV". *IEEE/OES autonomous underwater vehicles (AUV)*, pp.387–395
- [8] Yuh J., Li M, 2009, "Bioinspired Underwater Robots: Swimming Like the Fishes", *Bioinspiration & Biomimetics*, 4(1)
- [9] Craig.G. 2014 "Autonomous Underwater Vehicles: Technology and Applications", Annual Review of Control, Robotics, and Autonomous Systems.
- [10] Yingbo H and Yong Q 2003, "THAAD-like high altitude theatre missile defense: strategic defense capability and certain countermeasures analysis," *Science & Global Security*, 151–202
- [11] Sun M., Liang B., & Liu D. 2019. "Shape optimization design of a variable-section underwater vehicle control fin using a hybrid method" *Ocean Engineering*, 453-463
- [12] Wang G., Yu J., & Li H. 2018. "Multi-objective shape optimization for a novel AUV control fin using a hybrid surrogate model". *Ocean Engineering*, 170-182
- [13] Yu J. 2017, "Design and Control of a Biomimetic Ray-Inspired Flapping Underwater Vehicle", *IEEE Transactions on Robotics and Automation*
- [14] Zhao M., Li Z., & Lin P. 2017. "Hydrodynamic optimization design of a variable-section AUV hull using a multi-objective genetic algorithm" *Ocean Engineering*, 140, 147-159.
- [15] Y. Wang, G. Zhao, and D. Liu 2017 "Improving the hydrodynamic performance of an AUV using a bio-inspired design optimization method," *Ocean Engineering*, 327-339
- [16] M. Wang, Y. Liu, and Z. Zou 2016, "Multi-objective shape optimization of underwater vehicles using a hybrid PSO-SQP algorithm," *Ocean Engineering*, 222-233
- [17] G. Wu, H. Xu, and Z. Liu 2015, "Shape optimization of autonomous underwater vehicles using a hierarchical surrogate modelling approach," *Ocean Engineering*, 232-242
- [18] X. Liang, W. Lin, and H. Liu 2018 "Hydrodynamic design optimization of a wave-piercing catamaran AUV using a hybrid differential evolution algorithm," *Ocean Engineering*, 372-386.
- [19] G. Wu, H. Xu, and Z. Liu 2015, "Shape optimization of autonomous underwater vehicles using a hierarchical surrogate modeling approach," *Ocean Engineering*, 232-242.
- [20] Gao F., 2020 "Deep Reinforcement Learning for Autonomous Navigation of Underwater Vehicles in

Tuijin Jishu/Journal of Propulsion Technology

ISSN: 1001-4055 Vol. 45 No. 2 (2024)

Unknown Environments", IEEE Transactions on Cybernetics

- [21] Jain Gautam 2019, "A Study of Fiberglass Material with Different Compositions", SSRN Electronic Journal.
- [22] Wei Gao, Wenbin He, Wei Gong, Zhiqiang Liang, Zhimin Wang, 2013 "Multi-Objective Optimization of Control Fin Design for an Autonomous Underwater Vehicle" *IEEE Explore* 0197-7385.
- [23] Liu Y, Zou Z, and Lin W 2016, "A review of optimization methods for underwater vehicle design," *Ocean Engineering*, 100-112
- [24] Liang X, Lin W, and Liu H 2018 "Hydrodynamic shape optimization of an underwater glider using a surrogate-based differential evolution algorithm," *Ocean Engineering*, 507-520
- [25] Guo Y, Pan J, and Wu J 2019 "Design optimization of a wave glider for offshore wind farm inspection," *Ocean Engineering*,147-1 58.